








UCIP: A Universal Framework for Compressed Image Super-Resolution using Dynamic Prompt

Xin Li¹[†], Bingchen Li¹[†], Yeying Jin², Cuiling Lan³, Hanxin Zhu¹
Yulin Ren¹, and Zhibo Chen¹

¹ University of Science and Technology of China

² National University of Singapore

³ Microsoft Research Asia

{xin.li, chenzhibo}@ustc.edu.cn, {lbc31415926, hanxinzhu, renyulin}@mail.ustc.edu.cn, jinyeying@u.nus.edu, culan@microsoft.com

Abstract. Compressed Image Super-resolution (CSR) aims to simultaneously super-resolve the compressed images and tackle the challenging hybrid distortions caused by compression. However, existing works on CSR usually focus on single compression codec, *i.e.*, JPEG, ignoring the diverse traditional or learning-based codecs in the practical application, *e.g.*, HEVC, VVC, HIFIC, *etc.* In this work, we propose the first universal CSR framework, dubbed UCIP, with dynamic prompt learning, intending to jointly support the CSR distortions of any compression codecs/modes. Particularly, an efficient dynamic prompt strategy is proposed to mine the content/spatial-aware task-adaptive contextual information for the universal CSR task, using only a small amount of prompts with spatial size 1×1 . To simplify contextual information mining, we introduce the novel MLP-like framework backbone for our UCIP by adapting the Active Token Mixer (ATM) to CSR tasks for the first time, where the global information modeling is only taken in horizontal and vertical directions with offset prediction. We also build an all-in-one benchmark dataset for the CSR task by collecting the datasets with the popular 6 diverse traditional and learning-based codecs, including JPEG, HEVC, VVC, HIFIC, *etc.*, resulting in 23 common degradations. Extensive experiments have shown the consistent and excellent performance of our UCIP on universal CSR tasks. The project can be found in <https://lixinustc.github.io/UCIP.github.io>

Keywords: Dynamic Prompt · Universal Compressed Image SR · MLP-like framework

1 Introduction

In recent years, we have witnessed the significant development of Deep Neural Networks (DNNs) in image super-resolution (SR) [12, 24, 26, 31, 50, 60, 62, 63, 65, 71], where the image is degraded with low-resolution artifacts. However,

[†] Equal Contribution.

in the practical scenario, due to the limitation of storage and bandwidth, collected images are also inevitably compressed with traditional image codecs, such as JPEG [59], and BPG [49]. Accordingly, compressed image super-resolution (CSR) is proposed as an advanced task, which greatly meets the requirements of industry and human life. In general, the low-quality images in CSR are jointly degraded with compression artifacts, *e.g.*, block artifacts, ring effects, and low-resolution artifacts. The severe and heterogeneous degradation poses more challenges and high requirements for the CSR backbones. Moreover, in real applications, the compression codecs are usually diverse in different platforms, which urgently entails the Universal CSR model.

There are some pioneering works [10, 24, 26, 60] attempting to remove this hard degradation by improving the representation ability. The representative strategy is to design the CSR backbone with the Transformer, which profits from the self-attention module. For instance, Swin2SR [10] introduces the enhanced Swin Transformer [36, 37] (*i.e.*, SwinV2) to boost the restoration capability of the CSR backbone. HST [24] utilizes the hierarchical backbone to excavate multi-scale representation for CSR. Despite the transformer-based backbones having revealed strong recovery capability in CSR, the high computational cost of the transformer prevents its application and training optimization [10, 34]. Recently, Multi-layer perceptron (MLP) has demonstrated its potential to achieve the trade-off between the computational cost and global dependency modeling in the classification [8, 33, 54, 55, 64], benefiting from its efficient and effective token mixer strategies. Inspired by this, the first MLP-based framework MAXIM [56] in image processing is proposed, where the image tokens interact in global and local manners with multi-axis MLP, respectively. However, the above works only focus on single distortion removal, which lacks enough universality for CSR tasks.

In this work, we propose the first universal framework, dubbed UCIP, for CSR tasks with our dynamic prompt strategy based on an MLP-like module. It is noteworthy that the optimal contextual information obtained with the CSR network tends to vary with the content/spatial and degradation type, which entails the content-aware task-adaptive contextual information modeling capability. To achieve this, existing prompt-based IR [23, 29, 32, 45] methods have attempted to set multiple prompts with image size, lacking adaptability for various input sizes and leading to more computational cost. In contrast, our dynamic prompt strategy can not only achieve content-aware task-adaptive modulation but also own more applicability. Concretely, we propose the Dynamic Prompt generation Module (DPM), where a group of prompts with the size of $1 \times 1 \times C_p$ is set and C_p is the channel dimension. Then spatial-wise composable coefficients $H \times W \times C_p$ are generated with the distorted images, which guides the cooperation of these prompt bases to form the dynamic prompt with image size, thereby owning the content/spatial- and task-adaptive modulation capability.

Based on the powerful DPM, we can achieve the universal CSR framework by incorporating it into existing CSR backbones. However, in the commonly used Transformer backbone, contextual information modeling is achieved with the cost attention module, where any two tokens are required to interact. In

contrast, an active token mixer (ATM) [64] has been proposed for the MLP-like backbone to reduce the computational cost by implicitly achieving contextual information modeling in the horizontal and vertical directions with offset generation. However, no works explore the potential of this backbone on low-level vision tasks. Inspired by this, we propose the dynamic prompt-guided token mixer block (PTMB) by fusing the advantages of our DPM and ATM, where our DPM can guide the contextual information modeling process of the ATM by modulating the offset prediction and token mixer. Notably, only horizontal and vertical contextual modeling in ATMs lacks enough local information utilization. Consequently, we increase a local branch in PTMB with one 3×3 convolution. Based on PTMB, our UCIP can achieve efficient and excellent universal compressed image super-resolution for different codecs/modes.

To build the benchmark dataset for universal CSR tasks, we collected the datasets with 6 representative image codecs, including 3 traditional codecs and 3 learning-based codecs. Concretely, traditional codecs consist of JPEG [59], all-intra mode of HEVC [49], and VVC [5]. For learning-based codecs, to ensure the diversity of degradations, we select 3 codecs with different optimization objectives, *i.e.*, PSNR-oriented, SSIM-oriented, and GAN-based codecs. In this way, our database can cover the prominent compression types in recent industry and research fields. We have compared our UCIP and reproduced state-of-the-art methods on this benchmark, which showcases the superiority and robustness of our UCIP.

The contributions of this paper are listed as follows:

- We propose the first universal framework, *i.e.*, UCIP for the CSR tasks with our dynamic prompt strategy, intending to achieve the "all-in-one" for the CSR degradations with different codecs/modes.
- We propose the dynamic prompt-guided token mixer block (PTMB) by fusing the advantages of our proposed dynamic prompt generation module (DPM) and revised active token mixer (ATM), as the basic block for UCIP.
- We propose the first dataset benchmark for universal CSR tasks by collecting datasets with 6 prominent traditional and learning-based codecs, consisting of multiple compression degrees. This ensures the diversity of degradations in the benchmark dataset, thereby being reliable as the benchmark to measure different CSR methods.
- Extensive experiments on our universal CSR benchmark dataset have revealed the effectiveness of our proposed UCIP, which outperforms the recent state-of-the-art transformer-based methods with lower computational costs.

2 Related Works

2.1 Compressed Image Super-resolution

Compressed Image Super-resolution aims to tackle complicated hybrid distortions, including compression artifacts and low-resolution artifacts [7, 14, 21, 24, 26, 30, 66, 67]. The first challenge for this task was held in the AIM2022 [67], where

the image is first downsampled with the bicubic operation and then compressed with a JPEG codec. To solve this hard degradation, some works [10, 24, 26, 46] seek to utilize the Transformer-based architecture as their backbone. For instance, Swin2SR [10] eliminates the training instability and the requirements for large data for CSR by incorporating the Swin Transformer V2 to SwinIR [34]. HST [24] utilizes the multi-scale information flow and pre-training strategy [28] to enhance the restoration process with a hierarchical swin transformer. To further fuse the advantages of convolution and transformer, Qin *et al.* [46] proposes a dual-branch network, which achieves the consecutive interaction between the convolution branch and transformer branch. In contrast, to achieve the trade-off between the performance and computational cost, we aim to explore one efficient and effective framework for universal CSR problem.

2.2 MLP-like Models

As the alternative model for Transformer and Convolution Neural Networks (CNNs), MLP-like models [8, 18, 33, 51, 52, 54, 55, 64, 68, 70] have attracted great attention for their concise architectures. Typically, the noticeable success of MLP-like models stems from the well-designed token-mixing strategies [64]. The pioneering works, MLP-Mixer [54] and ResMLP [55] adopt two types of MLP layers, *i.e.*, channel-mixing MLP and token-mixing MLP, which are responsible for the channel and spatial information interaction. To simplify the token-mixing MLP, Hou *et al.* [18] and Tang *et al.* [51] decompose the token-mixing MLP into the horizontal and vertical token-mixing MLPs. Sequentially, As-MLP [33] introduces the two-axis token shift in different channels to achieve global token mixing. There are also several works that take the hand-craft windows to enlarge the receptive field for better spatial token mixing, *e.g.*, WaveMLP [52], and MorphMLP [70]. However, the token-mixing strategies in the above methods are restrictively fixed and lack flexibility and adaptability for different contents. To overcome this, ATM [64] is proposed to achieve the active token selection and mixing in each channel. Based on the progress of the above MLP-like models, MAXIM [56] is the first work to introduce the MLP-like model in low-level processing. However, the potential of MLP-like models is yet to be explored, as restoration model not only requires long-range token mixing but also demands efficient local feature extractions.

2.3 Prompt Learning

In the field of Natural Language Processing (NLP), prompt learning has emerged as a pivotal technique, particularly with the advent of transformer-based pre-trained models such as GPT [6, 43] and BERT [11]. Prompt learning involves providing models with specific textual cues that guide their processing of subsequent input, which helps models fast adapt to unseen tasks or applications. This approach has proven instrumental in directing models for task-specific outputs without necessitating extensive retraining or fine-tuning. Despite the success in NLP tasks, some researchers adopt prompt learning into vision tasks [2, 20, 22,

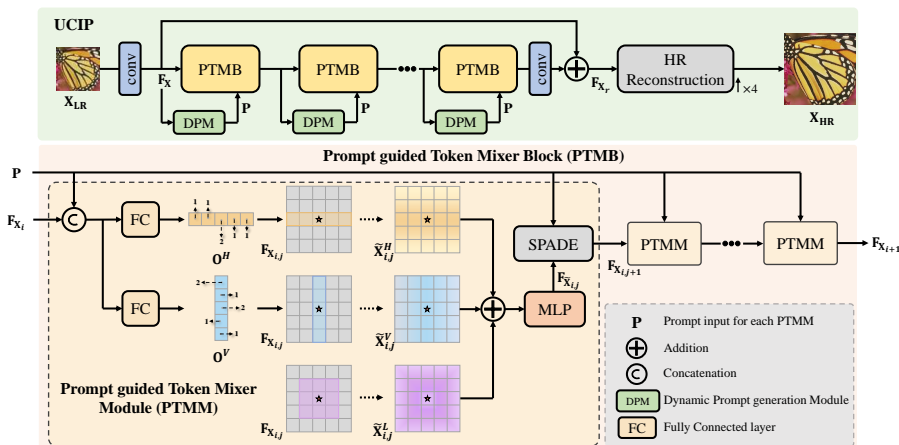


Fig. 1: Illustration of our proposed UCIP. From top to bottom: (a) The overall framework of UCIP. The LR is first enhanced through several consecutive PTMBs, then upsampled by HR reconstruction module. (b) The architecture of PTMB. Each PTMB utilizes the dynamic prompt generated from a DPM and several cascading PTMMs to iteratively refine distorted inputs. (c) The architecture of PTMM. PTMM takes prompt \mathbf{P} along with image feature \mathbf{F}_{x_i} as input to adaptively generate offsets, which facilitate the network to perform content/spatial-aware task-adaptive contextual information extraction.

27, 35, 47, 61]. Among them, PromptIR [45] is the first to explore the low-level restoration model with prompts to facilitate multi-task learning [13, 25, 48, 57, 58]. Prompts here act as a small set of learnable parameters which interact with image features during training, providing task-specific guidance. Therefore, the prompts should be as much dynamic as possible to adapt to various degradation tasks and different pixel distributions.

3 Methods

In this section, we first clarify the principle and construction of our dynamic prompt generation module in Sec. 3.1, and then describe how to achieve the basic block of our UCIP, *i.e.*, dynamic prompt-guided token mixer block in Sec. 3.2. Finally, we depict the whole framework of our UCIP in Sec. 3.3.

3.1 Dynamic Prompt Generation Module

As stated in Sec. 1, the universal CSR tasks entail the content/spatial- and task-adaptive modulation. An intuitive strategy is to set one prompt with the image size for each task individually or fuse them adaptively. However, it will bring severe parameter costs with the increase of the task number or image size [45]. To mitigate this, we propose the dynamic prompt strategy, and design

the corresponding dynamic prompt generation module (DPM), intending to only exploit a small amount of prompt with $1 \times 1 \times C_p$ and achieve the content/spatial- and task-adaptive with the cooperation of them. To this end, we decouple the large dynamic prompt with the size of $H \times W \times C_p$ into two smaller matrices, *i.e.*, the coefficients \mathbf{w}_I with the size of $H \times W \times D$ and D basic prompts with the size of $1 \times 1 \times C_p$. We can understand that for each spatial position $\{i, j\}$, there is one group of coefficients $w_I(i, j)$ to combine D basic prompts, thereby being content/spatial-adaptive. To let the dynamic prompt perceive the task information, we generate the coefficients with the feature of input images directly, thereby being task-adaptive and suitable for any input size. Our implementation has two advantages: 1) no extra operations to adjust the spatial size of prompts, and thus the guidance information from prompts is explicit and accurate; 2) our prompts have fewer parameters and are more computationally-friendly compared to previous methods [45].

The overall architecture of DPM is shown in Fig. 2, where the learnable basic prompts $\mathbf{P}_I \in \mathbb{R}^{D \times 1 \times 1 \times C_p}$ are set. Here, the D and C_p are the number of base prompts and the channel dimension of prompts. To generate dynamic prompt coefficients from input features $\mathbf{F}_X \in \mathbb{R}^{H \times W \times C}$, an MLP layer is applied to extract the degradation prior and transform the channel dimension from C to the number of basic prompts D . Then, the softmax operation is exploited to generate the composable coefficients $\mathbf{w}_I \in \mathbb{R}^{D \times H \times W \times 1}$ for basic prompts. Based on the inversion of the above dynamic prompt decomposition, we can obtain the dynamic prompt as:

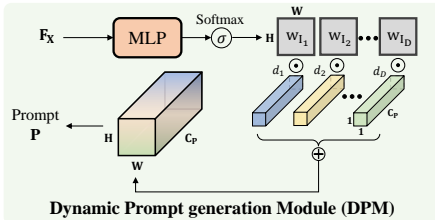


Fig. 2: The architecture of DPM. To dynamically aggregate content/spatial-aware task-adaptive contextual information, we introduce few number of basic dynamic kernels into the generation process of our prompt. Moreover, our design maintains adaptability to arbitrary input resolutions.

$$\mathbf{w}_I = \text{Softmax}(\text{MLP}(\mathbf{F}_X)), \quad \mathbf{P} = \sum^D (\mathbf{w}_I \odot \mathbf{P}_I) \quad (1)$$

3.2 Prompt-guided Token Mixer Block

Prompt-guided token mixer module After obtaining the dynamic prompt, we can exploit it to guide the restoration network for universal CSR tasks. Recently, Active Token Mixer (ATM) [64] gain great success in high-level vision tasks due to their well-designed token-mixing strategies. In contrast to transformer architecture, where the contextual information modeling is performed with the interactions between any two tokens, ATM utilize the deformable convolution to predict the offset of mostly relevant tokens, achieving the implicit contextual information modeling in the horizontal and vertical directions with offset generation.

Inspired by this, we propose the Dynamic Prompt-guided Token Mixer Module, dubbed PTMM by exploiting the dynamic prompt generated with DPM to guide the prediction of the offset of most informative tokens for contextual modeling. Concretely, PTMM leverages deformable convolutions and offsets to adaptively fuse tokens across horizontal and vertical axes, regardless of diverse degradation. However, as mentioned in [56], MLP-like modules exhibit diminished efficacy in the extraction of local relevance, which is essential for compressed super-resolution tasks. Therefore, we introduce a depth convolution around the target pixel to achieve the local information extraction.

As shown in Fig. 1(b), PTMM first extracts vertical and horizontal representative offsets $\mathbf{O}^V, \mathbf{O}^H$ by two sets of fully connected layers. To incorporate task-adaptive information during offset generation, we concatenate dynamic prompt generated from DPM with input features \mathbf{F}_X as the condition:

$$\mathbf{O}^{\{V,H\}} = \text{FC}_{\{V,H\}}(\text{Concat}([\mathbf{F}_X, \mathbf{P}])) \quad (2)$$

Then, we use the offset to recompose features along one certain axis into a new token $\tilde{\mathbf{x}}^{\{V,H\}}$ by the deformable convolution for information fusion (*i.e.*, token mixer). In addition, we adopt a depth convolution to achieve the local information extraction:

$$\tilde{\mathbf{x}}^L = \text{Conv}_{3 \times 3}(\mathbf{F}_X) \quad (3)$$

After we obtain these three tokens $\tilde{\mathbf{x}}^{\{V,H,L\}}$, we adaptively mix them with learned weights, formulated as

$$\mathbf{F}_{\tilde{\mathbf{x}}} = \boldsymbol{\alpha}^V \odot \tilde{\mathbf{x}}^V + \boldsymbol{\alpha}^H \odot \tilde{\mathbf{x}}^H + \boldsymbol{\alpha}^L \odot \tilde{\mathbf{x}}^L \quad (4)$$

where \odot denotes element-wise multiplication. $\boldsymbol{\alpha}^{\{V,H,L\}} \in \mathbb{R}^C$ are learned from the summation $\tilde{\mathbf{x}}^\Sigma$ of $\tilde{\mathbf{x}}^{\{V,H,L\}}$ with weights $W^{\{V,H,L\}} \in \mathbb{R}^{C \times C}$, where C denotes the channel dimension:

$$[\boldsymbol{\alpha}^V, \boldsymbol{\alpha}^H, \boldsymbol{\alpha}^L] = \sigma([W^V \cdot \tilde{\mathbf{x}}^\Sigma, W^H \cdot \tilde{\mathbf{x}}^\Sigma, W^L \cdot \tilde{\mathbf{x}}^\Sigma]),$$

Here, $\sigma(\cdot)$ is a softmax function for normalizing each channel separately.

To further incorporate the task prior for our UCIP, we modulate mixed features $\mathbf{F}_{\tilde{\mathbf{x}}}$ using the aforementioned dynamic prompt \mathbf{P} by a SPADE block [44] as the output features of the PTMM, which is shown in the Fig. 1.

Discussions There are two most relevant MLP-like methods, *i.e.*, MAXIM [56] and ActiveMLP [64]. The differences between MAXIM and our UCIP are as: MAXIM is only designed for specific task, where the cross-gating block and dense connection result in severe computational costs. The differences between ActiveMLP and our UCIP are as: ActiveMLP is designed for classification and focuses more on global information extraction, lacking local perception. Compared with them, our UCIP introduces the simple MLP-based architecture and the dynamic prompt for low-level vision, which is more applicable than the above methods for Universal CSR.

Overall pipeline To improve the modeling capability of PTMB, we connect N PTMMs in a successive way. It is worth noting that, to balance the performance of model and the computational cost, we share the prompt \mathbf{P} across all PTMMs within a single PTMB. With respect to offsets, we generate new offsets every two PTMMs. The whole process of PTMB can be formulated as:

$$\mathbf{P} = \text{DPM}(\mathbf{F}_X, \mathbf{P}_1), \quad \mathbf{F}_{X_{i+1}} = \text{PTMM}(\mathbf{P}, \mathbf{F}_{X_i}) \quad (5)$$

where \mathbf{F}_{X_i} is the input feature of i^{th} PTMM.

3.3 Overall Framework

As shown in Fig. 1, we build our UCIP following the popular pipeline of compressed super-resolution backbones, which is composed of shallow feature extraction, deep feature restoration, and HR reconstruction modules. Given a low-resolution input image $\mathbf{X}_{\text{LR}} \in \mathbb{R}^{H \times W \times 3}$, UCIP first extracts the shallow features $\mathbf{F}_X \in \mathbb{R}^{H \times W \times C}$ using a patch-embedding layer, where H , W are the spatial dimensions of features. Then, we pass \mathbf{F}_X through several PTMB to recursively remove the compression artifacts and generate the restored features \mathbf{F}_{X_r} . Finally, following [34, 63], we use a series of convolution layers and nearest interpolation operations to obtain the final high-resolution output \mathbf{X}_{HR} , which can be represented as:

$$\mathbf{X}_{\text{HR}} = \text{Conv}(\text{Conv}(\text{Conv}(\mathbf{F}_X + \mathbf{F}_{X_r}) \uparrow_{\times 2}) \uparrow_{\times 2}) \quad (6)$$

3.4 Our UCSR Dataset

To facilitate current and future research in CSR, we propose the first benchmark dataset for universal CSR, dubbed UCSR dataset, which not only considers traditional compression methods but also learning-based compression methods. We consider 6 types of compression codecs, including 3 most representative traditional codecs JPEG [59], HM [49], VTM [5], and 3 open-sourced learning-based codecs $\text{Cheng}_{\text{PSNR}}$ [9], $\text{Cheng}_{\text{SSIM}}$ [9] (abbreviated as C_{PSNR} and C_{SSIM} in the following paper), HIFIC [42]. These three learning-based codecs are PSNR-oriented and SSIM-oriented variants from [9] and perceptual-oriented GAN-based codecs from [42], respectively. To cover the prominent compression types in real scenarios, we consider four different compression qualities for each codec, except for HIFIC, since only the weights for three bitrate points are released.

To generate the training dataset, we choose the popular DF2K [1, 53], which contains 3450 high-quality images. Each image is downsampled by a scale factor of 4 using MATLAB bicubic algorithm. Then, we compress the downsampled images with six different compression algorithms to yield the training dataset of all competitive methods and our UCIP. The quality factors we used for different codecs are respectively as: (i) [10, 20, 30, 40] for JPEG, where the smaller value means poorer image quality. (ii) [32, 37, 42, 47] for HM, VTM, where value denotes the quantization parameter (QP), and larger value means poor quality. (iii) [1, 2, 3, 4] for C_{PSNR} , C_{SSIM} , where the smaller value indicates poorer

quality. We adopt the implementation in the popular open-sourced compression tools compressai [3]. (iv) [‘low’, ‘med’, ‘high’] for HIFIC, where ‘low’ indicates the poorest image quality. We use the PyTorch implementation [16] to compress images. All the methods are trained from scratch on our proposed benchmarks. We adopt the same process to generate the evaluation datasets based on five commonly used benchmarks: Set5 [4], Set14 [69], BSD100 [40], Urban100 [19] and Manga109 [41].

4 Experiments

Table 1: Quantitative comparison for compressed image super-resolution on traditional codecs. Results are tested on $\times 4$ with different compression qualities in terms of PSNR \uparrow /SSIM \uparrow . The best performances are in **red**. *Notably, all compared methods are trained from scratch with our proposed UCSR dataset for fair comparisons.* \mathcal{D} denotes for “Datasets”.

\mathcal{D}	Methods	JPEG [59]				HM [49]				VTM [5]			
		Q = 10	Q = 20	Q = 30	Q = 40	Q = 47	Q = 42	Q = 37	Q = 32	Q = 47	Q = 42	Q = 37	Q = 32
Set5 [4]	RRDB [63]	24.44/0.676	25.93/0.729	26.70/0.754	27.22/0.769	22.48/0.624	24.48/0.690	26.52/0.752	28.05/0.794	22.70/0.635	24.84/0.706	26.65/0.758	28.10/0.797
	SwinIR [34]	24.79/0.703	26.25/0.747	27.07/0.771	27.59/0.783	22.66/0.647	24.54/0.703	26.82/0.765	28.53/0.809	22.81/0.652	24.97/0.716	26.93/0.768	28.72/0.813
	Swin2SR [10]	24.80/0.705	26.24/0.752	27.16/0.774	27.64/0.786	22.66/0.650	24.55/0.705	26.81/0.766	28.50/0.809	22.79/0.652	24.91/0.716	26.89/0.769	28.64/0.813
	MAXIM [56]	24.83/0.709	26.15/0.751	27.00/0.773	27.44/0.784	22.69/0.648	24.60/0.705	26.75/0.764	28.48/0.808	22.88/0.654	24.96/0.718	26.89/0.770	28.61/0.811
	AIRNet [25]	24.67/0.701	26.04/0.745	26.83/0.767	27.30/0.779	22.56/0.640	24.38/0.698	26.55/0.760	28.24/0.805	22.71/0.648	24.81/0.714	26.65/0.766	28.38/0.810
	PromptIR [45]	24.82/0.707	26.24/0.751	27.13/0.774	27.62/0.787	22.68/0.652	24.55/0.705	26.87/0.768	28.64/0.813	22.89/0.658	24.99/0.720	26.93/0.771	28.74/0.815
UCIP	25.05/0.715	26.53/0.761	27.44/0.782	27.94/0.794	22.77/0.656	24.76/0.711	27.05/0.772	28.82/0.815	22.89/0.657	25.11/0.722	27.17/0.775	28.95/0.819	
Set14 [69]	RRDB [63]	23.40/0.579	24.49/0.619	25.01/0.639	25.32/0.651	21.84/0.531	23.48/0.584	24.93/0.635	25.99/0.679	22.12/0.541	23.74/0.594	25.09/0.643	26.05/0.682
	SwinIR [34]	23.77/0.596	24.81/0.630	25.32/0.649	25.66/0.662	21.96/0.542	23.59/0.593	25.13/0.645	26.38/0.695	22.19/0.550	23.79/0.599	25.32/0.652	26.49/0.699
	Swin2SR [10]	23.79/0.597	24.84/0.631	25.36/0.651	25.68/0.663	21.97/0.543	23.59/0.594	25.17/0.646	26.42/0.697	22.18/0.550	23.77/0.600	25.30/0.652	26.48/0.700
	MAXIM [56]	23.79/0.597	24.83/0.632	25.33/0.651	25.66/0.663	22.02/0.543	23.60/0.593	25.15/0.645	26.39/0.694	22.24/0.551	23.83/0.601	25.33/0.653	26.48/0.699
	AIRNet [25]	23.61/0.593	24.64/0.629	25.13/0.647	25.43/0.659	21.90/0.540	23.47/0.591	24.97/0.642	26.18/0.691	22.11/0.548	23.68/0.598	25.12/0.650	26.24/0.696
	PromptIR [45]	23.79/0.599	24.84/0.634	25.34/0.652	25.67/0.664	21.99/0.544	23.53/0.594	25.17/0.647	26.44/0.697	22.21/0.552	23.78/0.601	25.34/0.654	26.50/0.701
UCIP	23.93/0.602	24.99/0.637	25.53/0.657	25.88/0.669	22.10/0.547	23.70/0.597	25.34/0.650	26.63/0.701	22.28/0.553	23.89/0.603	25.45/0.656	26.71/0.705	
BSD100 [40]	RRDB [63]	23.56/0.547	24.44/0.580	24.86/0.597	25.12/0.609	22.10/0.503	23.43/0.542	24.64/0.588	25.58/0.630	22.30/0.510	23.64/0.550	24.80/0.595	25.66/0.634
	SwinIR [34]	23.79/0.557	24.62/0.587	25.04/0.604	25.31/0.616	22.17/0.510	23.45/0.548	24.74/0.596	25.80/0.643	22.34/0.516	23.66/0.555	24.91/0.603	25.92/0.649
	Swin2SR [10]	23.79/0.557	24.62/0.588	25.03/0.605	25.30/0.617	22.15/0.511	23.42/0.549	24.72/0.596	25.81/0.645	22.32/0.516	23.60/0.555	24.88/0.603	25.91/0.650
	MAXIM [56]	23.81/0.558	24.63/0.589	25.04/0.606	25.30/0.618	22.20/0.510	23.49/0.548	24.73/0.595	25.79/0.644	22.36/0.516	23.67/0.556	24.89/0.603	25.90/0.650
	AIRNet [25]	23.73/0.555	24.55/0.586	24.95/0.603	25.22/0.615	22.13/0.509	23.42/0.547	24.68/0.594	25.71/0.642	22.31/0.515	23.62/0.554	24.83/0.602	25.81/0.648
	PromptIR [45]	23.82/0.559	24.65/0.589	25.05/0.606	25.32/0.618	22.20/0.511	23.48/0.549	24.75/0.597	25.82/0.645	22.35/0.517	23.66/0.556	24.91/0.604	25.93/0.651
UCIP	23.88/0.561	24.73/0.593	25.15/0.610	25.42/0.623	22.24/0.513	23.56/0.551	24.84/0.599	25.93/0.649	22.38/0.517	23.74/0.558	24.99/0.606	26.03/0.654	
Urban100 [19]	RRDB [63]	21.69/0.578	22.18/0.597	22.66/0.622	22.97/0.638	20.42/0.531	21.66/0.578	22.84/0.633	23.61/0.671	20.67/0.543	21.95/0.593	23.00/0.641	23.66/0.674
	SwinIR [34]	21.74/0.580	22.61/0.621	23.11/0.646	23.41/0.661	20.45/0.535	21.86/0.595	23.18/0.654	24.12/0.699	20.70/0.546	22.10/0.607	23.33/0.662	24.19/0.703
	Swin2SR [10]	21.79/0.582	22.67/0.624	23.17/0.648	23.44/0.664	20.48/0.536	21.90/0.597	23.21/0.655	24.16/0.700	20.72/0.548	22.11/0.608	23.34/0.662	24.22/0.703
	MAXIM [56]	21.78/0.582	22.61/0.622	23.08/0.645	23.38/0.660	20.47/0.534	21.87/0.594	23.13/0.651	24.05/0.695	20.72/0.547	22.10/0.606	23.28/0.659	24.11/0.698
	AIRNet [25]	21.57/0.574	22.40/0.615	22.86/0.639	23.14/0.655	20.35/0.530	21.72/0.590	22.97/0.648	23.87/0.692	20.60/0.543	21.96/0.603	23.12/0.657	23.92/0.696
	PromptIR [45]	21.81/0.587	22.65/0.626	23.12/0.649	23.42/0.664	20.50/0.539	21.89/0.598	23.17/0.656	24.13/0.701	20.73/0.550	22.11/0.609	23.32/0.663	24.18/0.704
UCIP	22.00/0.596	22.88/0.637	23.39/0.664	23.71/0.677	20.59/0.542	22.05/0.604	23.39/0.661	24.42/0.711	20.80/0.552	22.23/0.614	23.50/0.670	24.46/0.715	
Manga109 [41]	RRDB [63]	22.50/0.684	23.75/0.730	24.49/0.756	24.99/0.773	21.17/0.655	23.24/0.722	25.07/0.778	26.24/0.813	21.59/0.675	23.64/0.738	25.27/0.786	26.29/0.815
	SwinIR [34]	23.05/0.720	24.38/0.762	25.16/0.786	25.67/0.801	21.40/0.677	23.56/0.743	25.64/0.801	27.17/0.841	21.73/0.689	23.90/0.754	25.83/0.807	27.25/0.843
	Swin2SR [10]	23.09/0.720	24.40/0.762	25.18/0.786	25.69/0.801	21.42/0.677	23.58/0.743	25.62/0.799	27.11/0.839	21.75/0.690	23.90/0.753	25.78/0.804	27.19/0.841
	MAXIM [56]	23.11/0.722	24.41/0.762	25.17/0.786	25.65/0.800	21.41/0.675	23.55/0.740	25.56/0.797	27.05/0.836	21.74/0.688	23.89/0.752	25.76/0.803	27.13/0.838
	AIRNet [25]	22.82/0.714	24.07/0.754	24.78/0.778	25.26/0.793	21.25/0.670	23.34/0.735	25.29/0.793	26.69/0.833	21.59/0.684	23.67/0.747	25.47/0.800	26.74/0.835
	PromptIR [45]	23.15/0.726	24.48/0.767	25.23/0.789	25.71/0.804	21.41/0.681	23.59/0.746	25.62/0.801	27.15/0.841	21.73/0.692	23.90/0.755	25.80/0.807	27.21/0.843
UCIP	23.36/0.734	24.77/0.775	25.58/0.798	26.11/0.813	21.54/0.683	23.79/0.750	25.94/0.808	27.61/0.848	21.82/0.693	24.06/0.759	26.08/0.812	27.68/0.850	

Our objective is to develop an MLP-like model that caters to a wide range of compressed image super-resolution tasks. Thus, we evaluate our UCIP on six different CSR tasks, including three traditional compression codecs: JPEG [59], HM [49], VTM [5]; and three learning-based compression codecs: C_{PSNR} [9], C_{SSIM} [9], HIFIC [42].

Implement details We train our UCIP from scratch in an end-to-end manner. We employ an Adam optimizer with initial learning rate of $3e-4$. The learning

rate is halved after 200k iterations, and the total number of iterations is set to 40w. The network is optimized by L1 loss. During training, we randomly cropped degraded low-resolution images into patches of size 64×64 , and 256×256 for high-resolution counterparts as well. Following previous works, random horizontal and vertical flips are utilized to augment training data. The total batch size is set to 32. For our baseline model, we use 6 PTMBs for UCIP and 6 PTMMs for each PTMB.

Training details To ensure fair comparisons, we train all the competitive methods following their official released codes on our proposed CSR training dataset with the same batch size. The performance are evaluated under the same training iterations.

4.1 Comparisons with State-of-the-arts

We evaluate UCIP with six state-of-the-art models on our CSR benchmarks which composes of five commonly adopted datasets: Set5 [4], Set14 [69], BSD100 [40], Urban100 [19] and Manga109 [41]. The compared models include the fully-convolutional network RRDB [63], the transformer-based image restoration model SwinIR [34] and its upgraded version Swin2SR [10], the MLP-like model MAXIM [56] and two multi-task models AIRNet [25] and PromptIR [45]. We add the HR reconstruction module to last three models, enabling them to perform super-resolution tasks. *All compared methods are trained from scratch with our proposed UCSR dataset for fair comparisons.*

As demonstrated in Table. 1 and Table. 2, our UCIP outperforms all other methods on almost all codecs and compression qualities. Particularly, UCIP achieves PSNR gain of up to 0.45dB against PromptIR [45] with only one-third the number of parameters. Another intriguing observation is that the gains provided by UCIP become more significant as the compression ratio decreases. We attribute this to the preservation of more high-frequency information at milder compression levels. The abundance of high-frequency details further enhances the capability of PTMM to conduct global-wise informative tokens extraction, thus leads to a better performance.

As illustrated in Fig. 3, UCIP leverages the implicit guidance of the dynamic prompt to recover more textural details while avoiding the generation of artifacts. Specifically, as observed in the first row, our model recovers the clearest texture of the monarch. Besides, in the second and final rows, images reconstructed by our method exhibit clearer edges and fewer distorted lines. For the third row, our method successfully removes compression artifacts, while other methods suffer from blocked and blurry outputs. We attribute these performances to the generation of the dynamic prompt and the fusion of global tokens with local features.

It is noteworthy that, though we do not specifically tailor prompts for various compression qualities within certain codec, experimental evidence suggests that our dynamic prompt not only possesses task-specific adaptability but is also

Table 2: Quantitative comparison for compressed image super-resolution on learning-based codecs. Results are tested on $\times 4$ with different compression qualities in terms of PSNR \uparrow /SSIM \uparrow . The best performances are in red. Notice that, as HIFIC [42] does not support some low-resolution images from downsampled Set5 and Set14 datasets, we do not use HIFIC codec to compress these two datasets. *Notably, all compared methods are trained from scratch with our proposed UCSR dataset for fair comparisons.* \mathcal{D} denotes for ‘‘Datasets’’.

\mathcal{D}	Methods	Params	C _{PSNR} [9]				C _{SSIM} [9]				HIFIC [42]		
			Q = 1	Q = 2	Q = 3	Q = 4	Q = 1	Q = 2	Q = 3	Q = 4	Q = ‘low’	Q = ‘med’	Q = ‘high’
Set5 [4]	RRDB [63]	16.70M	24.54/0.698	25.40/0.725	26.14/0.746	27.37/0.781	21.19/0.591	21.91/0.621	22.94/0.654	23.69/0.684	-	-	-
	SwinIR [34]	11.72M	24.55/0.704	25.50/0.731	26.25/0.753	27.70/0.790	21.19/0.595	21.93/0.629	22.96/0.663	23.70/0.689	-	-	-
	Swin2SR [10]	12.05M	24.56/0.702	25.51/0.732	26.27/0.756	27.69/0.792	21.23/0.595	21.95/0.629	22.98/0.662	23.77/0.691	-	-	-
	MAXIM [56]	26.74M	24.58/0.704	25.49/0.733	26.27/0.755	27.66/0.791	21.26/0.595	22.01/0.631	23.03/0.663	23.78/0.692	-	-	-
	AIRNet [25]	7.76M	24.54/0.702	25.41/0.730	26.16/0.751	27.50/0.789	21.15/0.595	21.91/0.629	22.93/0.660	23.67/0.689	-	-	-
	PromptIR [45]	35.72M	24.48/0.700	25.42/0.730	26.16/0.751	27.72/0.793	21.26/0.600	21.99/0.632	22.98/0.661	23.66/0.686	-	-	-
UCIP	11.42M	24.65/0.705	25.59/0.736	26.39/0.758	27.93/0.796	21.30/0.607	21.98/0.633	23.01/0.663	23.74/0.689	-	-	-	
Set14 [69]	RRDB [63]	16.70M	23.52/0.588	24.17/0.611	24.76/0.632	25.51/0.662	21.19/0.526	21.70/0.545	22.38/0.564	23.04/0.586	-	-	-
	SwinIR [34]	11.72M	23.61/0.591	24.29/0.615	24.92/0.638	25.82/0.673	21.20/0.527	21.69/0.545	22.39/0.566	23.03/0.587	-	-	-
	Swin2SR [10]	12.05M	23.61/0.591	24.29/0.615	24.91/0.638	25.82/0.673	21.20/0.527	21.72/0.546	22.40/0.566	23.05/0.587	-	-	-
	MAXIM [56]	26.74M	23.61/0.592	24.31/0.615	24.94/0.639	25.82/0.673	21.23/0.527	21.75/0.546	22.42/0.565	23.10/0.588	-	-	-
	AIRNet [25]	7.76M	23.53/0.590	24.19/0.614	24.82/0.637	25.65/0.672	21.14/0.526	21.66/0.545	22.35/0.565	23.00/0.587	-	-	-
	PromptIR [45]	35.72M	23.62/0.592	24.30/0.616	24.95/0.639	25.85/0.675	21.20/0.528	21.73/0.547	22.43/0.566	23.08/0.588	-	-	-
UCIP	11.42M	23.66/0.593	24.34/0.617	25.00/0.641	25.97/0.678	21.24/0.529	21.73/0.547	22.41/0.567	23.10/0.590	-	-	-	
BSD100 [40]	RRDB [63]	16.70M	23.55/0.548	24.15/0.569	24.67/0.590	25.27/0.618	21.95/0.507	22.44/0.523	23.07/0.540	23.53/0.556	21.27/0.521	21.99/0.550	22.38/0.575
	SwinIR [34]	11.72M	23.58/0.549	24.19/0.573	24.73/0.595	25.42/0.627	21.95/0.508	22.45/0.524	23.07/0.541	23.54/0.557	21.46/0.531	22.11/0.556	22.59/0.581
	Swin2SR [10]	12.05M	23.57/0.550	24.19/0.573	24.71/0.595	25.39/0.627	21.95/0.507	22.44/0.524	23.07/0.541	23.53/0.557	21.44/0.531	22.12/0.557	22.55/0.582
	MAXIM [56]	26.74M	23.59/0.550	24.20/0.573	24.74/0.595	25.42/0.628	21.97/0.508	22.47/0.524	23.10/0.541	23.56/0.557	21.51/0.531	22.17/0.557	22.54/0.580
	AIRNet [25]	7.76M	23.56/0.549	24.16/0.573	24.70/0.595	25.36/0.627	21.95/0.507	22.44/0.524	23.05/0.541	23.51/0.557	21.44/0.530	22.11/0.556	22.51/0.579
	PromptIR [45]	35.72M	23.59/0.550	24.21/0.573	24.75/0.596	25.43/0.628	21.96/0.508	22.47/0.524	23.09/0.541	23.55/0.558	21.49/0.532	22.14/0.558	22.66/0.583
UCIP	11.42M	23.61/0.551	24.24/0.575	24.77/0.597	25.49/0.630	21.98/0.508	22.48/0.525	23.12/0.543	23.59/0.560	21.94/0.534	22.19/0.559	23.39/0.587	
Urban100 [19]	RRDB [63]	16.70M	21.70/0.580	22.21/0.603	22.60/0.622	23.21/0.654	19.84/0.504	20.29/0.524	20.81/0.546	21.31/0.570	20.70/0.540	21.42/0.570	21.89/0.593
	SwinIR [34]	11.72M	21.78/0.587	22.32/0.613	22.76/0.633	23.52/0.672	19.87/0.509	20.31/0.530	20.86/0.553	21.36/0.579	20.83/0.549	21.60/0.579	22.11/0.605
	Swin2SR [10]	12.05M	21.82/0.588	22.38/0.614	22.80/0.635	23.52/0.672	19.89/0.510	20.33/0.531	20.89/0.554	21.41/0.580	20.87/0.550	21.65/0.580	22.16/0.607
	MAXIM [56]	26.74M	21.80/0.587	22.34/0.612	22.77/0.633	23.49/0.670	19.90/0.509	20.35/0.530	20.89/0.553	21.40/0.578	20.87/0.549	21.63/0.579	22.14/0.605
	AIRNet [25]	7.76M	21.71/0.585	22.23/0.610	22.65/0.631	23.34/0.668	19.84/0.507	20.27/0.527	20.81/0.550	21.30/0.575	20.77/0.546	21.49/0.576	21.98/0.600
	PromptIR [45]	35.72M	21.82/0.589	22.35/0.614	22.79/0.635	23.53/0.673	19.92/0.511	20.36/0.532	20.91/0.555	21.42/0.581	20.88/0.552	21.64/0.583	22.19/0.610
UCIP	11.42M	21.89/0.593	22.46/0.620	22.91/0.641	23.72/0.682	19.98/0.516	20.43/0.538	21.01/0.563	21.56/0.590	20.95/0.555	21.77/0.588	22.30/0.616	
Manga098 [41]	RRDB [63]	16.70M	23.20/0.725	23.90/0.746	24.43/0.762	25.47/0.794	20.12/0.635	20.75/0.657	21.55/0.680	22.27/0.705	21.28/0.671	22.41/0.705	23.10/0.729
	SwinIR [34]	11.72M	23.31/0.733	24.13/0.760	24.68/0.775	26.01/0.813	20.12/0.641	20.75/0.664	21.58/0.689	22.34/0.715	21.32/0.680	22.55/0.716	23.31/0.742
	Swin2SR [10]	12.05M	23.33/0.733	24.08/0.757	24.68/0.774	25.91/0.809	20.15/0.641	20.79/0.664	21.62/0.689	22.38/0.715	21.36/0.679	22.61/0.715	23.37/0.742
	MAXIM [56]	26.74M	23.31/0.732	24.08/0.756	24.67/0.774	25.95/0.810	20.15/0.640	20.78/0.663	21.60/0.687	22.34/0.712	21.36/0.679	22.58/0.715	23.33/0.741
	AIRNet [25]	7.76M	23.17/0.729	23.89/0.752	24.47/0.770	25.66/0.807	20.08/0.637	20.70/0.660	21.49/0.684	22.22/0.709	21.33/0.676	22.42/0.711	23.18/0.736
	PromptIR [45]	35.72M	23.33/0.734	24.09/0.758	24.70/0.775	25.97/0.812	20.15/0.642	20.79/0.665	21.62/0.690	22.36/0.715	21.39/0.682	22.58/0.718	23.40/0.745
UCIP	11.42M	23.43/0.737	24.24/0.762	24.88/0.781	26.29/0.819	20.19/0.645	20.85/0.669	21.73/0.696	22.53/0.723	21.41/0.684	22.70/0.723	23.55/0.750	

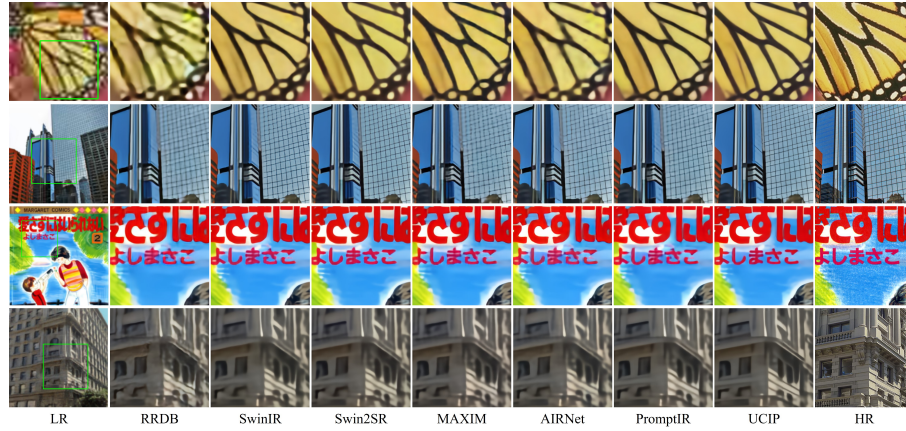


Fig. 3: Visual comparisons between UCIP and other state-of-the-art methods. To demonstrate the effectiveness of UCIP across different codecs, we display four rows of images, each compressed with JPEG ($Q = 10$), HM ($Q = 32$), C_{PSNR} ($Q = 4$) and HIFIC ($Q = \text{‘med’}$), respectively. We show more results in the Sec. 7.

capable of handling different distortion degrades. As shown in Fig. 4, our method maintains robust image restoration capabilities across three levels of compression qualities (*e.g.*, always recovers straight lines on the right side of image).

Table 3: Quantitative comparison for different tuning methods on two new codecs. Results are tested on $\times 4$ with different compression qualities in terms of PSNR \uparrow /SSIM \uparrow . **The first line of each benchmark denotes the baseline model trained with our proposed UCSR dataset, which is directly evaluated on these new codecs.** Notice that, for both codecs, the smaller the quality factor, the poorer the image quality. The best performances are in **red**. Zoom in for best view.

Datasets	Pre-train with prompts	Add prompts in fine-tune	Fine-tune which part	WebP [15]				ELIC [17]			
				Q = 10	Q = 20	Q = 30	Q = 40	Q = 1	Q = 2	Q = 3	Q = 4
Set5	-	-	-	26.20/0.750	27.12/0.777	27.78/0.794	28.33/0.806	22.48/0.643	23.51/0.677	24.63/0.708	25.55/0.735
	\times	\checkmark	only prompts	26.25/0.753	27.16/0.778	27.83/0.795	28.40/0.809	22.43/0.639	23.57/0.678	24.81/0.713	25.97/0.745
	\times	\checkmark	full model	26.55/0.763	27.49/0.787	28.20/0.805	28.79/0.818	22.41/0.642	23.53/0.678	24.83/0.716	26.06/0.749
	\checkmark	\checkmark	only prompts	26.54/0.762	27.49/0.787	28.18/0.804	28.78/0.818	22.42/0.644	23.55/0.679	24.84/0.715	26.03/0.748
Set14	-	-	-	24.69/0.631	25.41/0.658	25.87/0.675	26.25/0.689	21.84/0.539	22.78/0.566	23.62/0.593	24.37/0.618
	\times	\checkmark	only prompts	24.76/0.634	25.43/0.659	25.91/0.678	26.29/0.693	21.86/0.540	22.81/0.567	23.69/0.595	24.58/0.625
	\times	\checkmark	full model	24.93/0.641	25.64/0.667	26.12/0.686	26.53/0.701	21.85/0.541	22.81/0.569	23.73/0.597	24.67/0.628
	\checkmark	\checkmark	only prompts	24.97/0.642	25.65/0.668	26.14/0.686	26.55/0.701	21.84/0.540	22.81/0.568	23.73/0.597	24.69/0.629
BSD100	-	-	-	24.36/0.583	24.93/0.608	25.34/0.626	25.63/0.639	22.14/0.507	22.90/0.528	23.61/0.551	24.20/0.574
	\times	\checkmark	only prompts	24.44/0.587	25.01/0.612	25.42/0.630	25.74/0.644	22.12/0.508	22.89/0.529	23.63/0.553	24.33/0.580
	\times	\checkmark	full model	24.55/0.592	25.11/0.616	25.52/0.635	25.85/0.649	22.10/0.509	22.88/0.530	23.64/0.554	24.36/0.581
	\checkmark	\checkmark	only prompts	24.55/0.593	25.11/0.617	25.53/0.636	25.86/0.650	22.10/0.509	22.89/0.530	23.64/0.554	24.37/0.582
Urban100	-	-	-	22.81/0.640	23.43/0.669	23.81/0.687	24.07/0.698	20.49/0.533	21.32/0.569	22.00/0.602	22.54/0.629
	\times	\checkmark	only prompts	22.72/0.634	23.30/0.661	23.67/0.679	23.94/0.691	20.48/0.532	21.31/0.568	22.05/0.601	22.70/0.632
	\times	\checkmark	full model	23.06/0.653	23.66/0.680	24.05/0.698	24.34/0.710	20.47/0.535	21.33/0.572	22.10/0.607	22.81/0.640
	\checkmark	\checkmark	only prompts	23.15/0.656	23.74/0.683	24.13/0.701	24.41/0.713	20.54/0.538	21.40/0.575	22.18/0.610	22.88/0.643
Manga109	-	-	-	24.77/0.779	25.69/0.805	26.28/0.820	26.70/0.831	21.20/0.671	22.36/0.707	23.36/0.739	24.22/0.766
	\times	\checkmark	only prompts	24.76/0.776	25.65/0.801	26.23/0.817	26.66/0.828	21.22/0.671	22.42/0.708	23.52/0.741	24.60/0.774
	\times	\checkmark	full model	25.09/0.789	26.01/0.813	26.65/0.829	27.16/0.841	21.19/0.670	22.42/0.711	23.58/0.746	24.73/0.780
	\checkmark	\checkmark	only prompts	25.18/0.791	26.11/0.815	26.75/0.831	27.25/0.843	21.23/0.675	22.48/0.713	23.65/0.747	24.82/0.783

4.2 Prompt Tuning for UCIP

Prompt learning can be utilized in two popular ways: (i) One is to utilize prompt learning for multi-task learning, *e.g.*, PromptIR [45], ProRes [39], PIP [32] in low-level vision, which needs to train whole model from scratch; (ii) another is prompt tuning, which requires a strong baseline model and aims to optimize only a small part of parameters for downstream tasks. Notably, in the CSR field, there are no pre-trained baseline models on multiple types of compression artifacts existed, which prevents us to study prompt tuning in the beginning. And thus, we build the first Universal CSR framework and corresponding dataset with the first way, which follows existing prompt learning works in low-level vision [32, 38, 39, 45]. However, training a model from scratch is time consuming. To further explore the potential of our proposed UCIP in prompt tuning, we choose two *unseen* codecs, including one traditional codec WebP [15] and one learning-based codec ELIC [17], to fine-tune UCIP. In Tab. 3, we explore four ways of fine-tuning: i) directly evaluated pre-trained model without fine-tuning. ii) pre-training without prompt, then adding prompt and only training prompt parameters on new tasks. iii) pre-training without prompt, then adding prompt and only training prompt parameters on new tasks. iv) pre-training with prompt, then fine-tuning only prompt parameters on new tasks. All the experiments are conducted under the

same settings with the same training iterations. As shown in Tab. 3, compared between ii) and iii), tuning only prompt achieves comparable performance on ELIC codec against tuning full model. Compared between iii) and iv), tuning only prompt based on UCIP achieves comparable and even better performances against tuning full model after adding prompt. The experimental results indicate that our proposed UCIP can serve as a strong baseline model in CSR field, which will also benefit the prompt tuning for new codecs in future works.

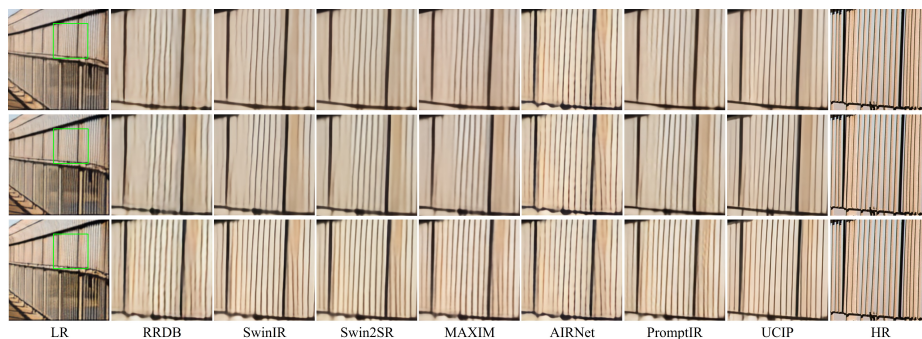


Fig. 4: Visual comparisons between UCIP and other state-of-the-art methods under different compression qualities within HIFIC [42] codec. The qualities of HIFIC from top to bottom are ‘low’, ‘medium’, and ‘high’, respectively. We show more results in the Sec. 7.

4.3 Ablation Studies

The effects of dynamic prompt To validate the effectiveness of our DPM, we conduct experiments on the different prompt designs. The results are shown in Table. 4. Specifically, without the dynamic prompt, UCIP is unable to perform task-wise informative token selection. Moreover, the use of fixed prompts may even impair the performance of UCIP, as they could provide incorrect guidance during the token mixing process. Compared to PromptIR [45], our DPM utilizes very few parameters to achieve the spatial-adaptive modulation for tasks by only a few basic dynamic prompt kernels, thereby achieving a PSNR gain of up to 0.22dB.

The effects of local feature extraction As demonstrated in Sec. 3.2, local feature extraction is essential for the model to aggregate useful local information with the content/spatial-aware task-adaptive contextual information. To validate this point, we conduct an ablation which replaces the local convolution with the identity module. As shown in Table. 5, PSNR drops about 0.1dB without local feature extraction, which indicates that incorporate global tokens with local features are necessary for CSR tasks.

Table 4: Impacts of different prompt generation strategies. Results are reported on Manga109 [41]. Flops is calculated based on input with the size $1 \times 3 \times 64 \times 64$.

Method	Params(M)	Flops(G)	Codecs		
			JPEG(Q = 40)	HM(Q = 32)	HIFIC(Q = 'high')
w/o Prompt	-	-	25.70/0.805	27.22/0.840	23.39/0.745
Fixed	-	-	25.62/0.799	27.10/0.839	23.05/0.723
PromptIR [45]	9.66	0.900	25.89/0.810	27.42/0.845	23.50/0.749
Ours	0.46	0.024	26.11/0.813	27.61/0.848	23.55/0.750

Table 5: Impacts of local feature extraction. Results are reported on Manga109 [41].

Codecs	Methods	
	w/o Conv _{3×3}	Ours
JPEG(Q = 40)	25.97/0.809	26.11/0.813
HM(Q = 32)	27.46/0.844	27.61/0.848
HIFIC(Q = 'high')	23.48/0.747	23.55/0.750

Table 6: Experiments about number of the dynamic prompt. Results are reported on Manga109 [41].

Number	Codecs		
	JPEG(Q = 40)	HM(Q = 32)	HIFIC(Q = 'high')
1	25.84/0.807	27.42/0.844	23.46/0.747
2	25.88/0.808	27.42/0.845	23.48/0.748
4	25.99/0.811	27.53/0.847	23.52/0.748
8(Ours)	26.11/0.813	27.61/0.848	23.55/0.750
16	26.19/0.815	27.66/0.850	23.59/0.751

The effects of number of the dynamic prompt To mine the content/spatial-aware task-adaptive contextual information for the universal CSR task, we introduce the dynamic prompt. In this part, we investigate the optimal number of the dynamic prompt. As demonstrated in Table 6, there is a noticeable constraint on the dynamic capacity of prompts for spatial content interpretation and degradation handling when the number of the dynamic prompt is small. As the number incrementally increases, the observed performance gap narrows, falling below our expectations. We attribute this to the inadequate weighting from input image features, primarily due to the constrained capabilities of a singular MLP layer. To strike a balance between performance and computational efficiency, we choose 8 as the number of the dynamic prompt.

5 Conclusion

In this paper, we present UCIP, the first universal Compressed Image Super-resolution model, which leverages a novel dynamic prompt structure with multi-layer perception (MLP)-like framework. Distinct from existing CSR works focused on a single compression codec JPEG, UCIP effectively addresses hybrid distortions across a spectrum of codecs. By utilizing the prompt-guided token mixer block (PTMB), it dynamically identifies and refines the content/spatial-aware task-adaptive contextual information, optimizing for different tasks and distortions. Our extensive experiments on the proposed comprehensive UCSR benchmarks confirm that UCIP not only achieves state-of-the-art performance but also demonstrates remarkable versatility and applicability. In future work, we will exploit the potential of UCIP and further improve both objective and subjective performances on UCSR benchmarks.

Acknowledgement

This work was supported in part by NSFC under Grant 623B2098, 62021001, and 62371434. This work was mainly completed before March 2024.

References

1. Agustsson, E., Timofte, R.: Ntire 2017 challenge on single image super-resolution: Dataset and study. In: Proceedings of the IEEE conference on computer vision and pattern recognition workshops. pp. 126–135 (2017)
2. Ai, Y., Huang, H., Zhou, X., Wang, J., He, R.: Multimodal prompt perceiver: Empower adaptiveness, generalizability and fidelity for all-in-one image restoration. arXiv preprint arXiv:2312.02918 (2023)
3. Bégaint, J., Racapé, F., Feltman, S., Pushparaja, A.: Compressai: a pytorch library and evaluation platform for end-to-end compression research. arXiv preprint arXiv:2011.03029 (2020)
4. Bevilacqua, M., Roumy, A., Guillemot, C., Alberi-Morel, M.L.: Low-complexity single-image super-resolution based on nonnegative neighbor embedding (2012)
5. Bross, B., Wang, Y.K., Ye, Y., Liu, S., Chen, J., Sullivan, G.J., Ohm, J.R.: Overview of the versatile video coding (vvc) standard and its applications. IEEE Transactions on Circuits and Systems for Video Technology **31**(10), 3736–3764 (2021)
6. Brown, T., Mann, B., Ryder, N., Subbiah, M., Kaplan, J.D., Dhariwal, P., Neelakantan, A., Shyam, P., Sastry, G., Askell, A., et al.: Language models are few-shot learners. Advances in neural information processing systems **33**, 1877–1901 (2020)
7. Chen, H., Wang, Y., Guo, T., Xu, C., Deng, Y., Liu, Z., Ma, S., Xu, C., Xu, C., Gao, W.: Pre-trained image processing transformer. In: Proceedings of the IEEE/CVF conference on computer vision and pattern recognition. pp. 12299–12310 (2021)
8. Chen, S., Xie, E., Ge, C., Liang, D., Luo, P.: Cyclemlp: A mlp-like architecture for dense prediction. arXiv preprint arXiv:2107.10224 (2021)
9. Cheng, Z., Sun, H., Takeuchi, M., Katto, J.: Learned image compression with discretized gaussian mixture likelihoods and attention modules. In: Proceedings of the IEEE/CVF conference on computer vision and pattern recognition. pp. 7939–7948 (2020)
10. Conde, M.V., Choi, U.J., Burchi, M., Timofte, R.: Swin2sr: Swinv2 transformer for compressed image super-resolution and restoration. arXiv preprint arXiv:2209.11345 (2022)
11. Devlin, J., Chang, M.W., Lee, K., Toutanova, K.: Bert: Pre-training of deep bidirectional transformers for language understanding. arXiv preprint arXiv:1810.04805 (2018)
12. Fritsche, M., Gu, S., Timofte, R.: Frequency separation for real-world super-resolution. In: 2019 IEEE/CVF International Conference on Computer Vision Workshop (ICCVW). pp. 3599–3608. IEEE (2019)
13. Gao, H., Yang, J., Wang, N., Yang, J., Zhang, Y., Dang, D.: Prompt-based all-in-one image restoration using cnns and transformer. arXiv preprint arXiv:2309.03063 (2023)
14. Gao, W., Tao, L., Zhou, L., Yang, D., Zhang, X., Guo, Z.: Low-rate image compression with super-resolution learning. In: Proceedings of the IEEE/CVF Conference on Computer Vision and Pattern Recognition Workshops. pp. 154–155 (2020)

15. Google: Web picture format. <https://chromium.googlesource.com/webm/libwebp>, (2010)
16. Grace Han, J.T.: high-fidelity-generative-compression. <https://github.com/Justin-Tan/high-fidelity-generative-compression>, (2020)
17. He, D., Yang, Z., Peng, W., Ma, R., Qin, H., Wang, Y.: Elic: Efficient learned image compression with unevenly grouped space-channel contextual adaptive coding. In: Proceedings of the IEEE/CVF Conference on Computer Vision and Pattern Recognition. pp. 5718–5727 (2022)
18. Hou, Q., Jiang, Z., Yuan, L., Cheng, M.M., Yan, S., Feng, J.: Vision permutator: A permutable mlp-like architecture for visual recognition. *IEEE Transactions on Pattern Analysis and Machine Intelligence* **45**(1), 1328–1334 (2022)
19. Huang, J.B., Singh, A., Ahuja, N.: Single image super-resolution from transformed self-exemplars. In: Proceedings of the IEEE conference on computer vision and pattern recognition. pp. 5197–5206 (2015)
20. Jia, M., Tang, L., Chen, B.C., Cardie, C., Belongie, S., Hariharan, B., Lim, S.N.: Visual prompt tuning. In: European Conference on Computer Vision. pp. 709–727. Springer (2022)
21. Jiang, J., Zhang, K., Timofte, R.: Towards flexible blind jpeg artifacts removal. In: Proceedings of the IEEE/CVF International Conference on Computer Vision. pp. 4997–5006 (2021)
22. Kong, X., Dong, C., Zhang, L.: Towards effective multiple-in-one image restoration: A sequential and prompt learning strategy. arXiv preprint arXiv:2401.03379 (2024)
23. Li, B., Li, X., Lu, Y., Feng, R., Guo, M., Zhao, S., Zhang, L., Chen, Z.: Prompt-cir: Blind compressed image restoration with prompt learning. arXiv preprint arXiv:2404.17433 (2024)
24. Li, B., Li, X., Lu, Y., Liu, S., Feng, R., Chen, Z.: Hst: Hierarchical swin transformer for compressed image super-resolution. arXiv preprint arXiv:2208.09885 (2022)
25. Li, B., Liu, X., Hu, P., Wu, Z., Lv, J., Peng, X.: All-in-one image restoration for unknown corruption. In: Proceedings of the IEEE/CVF Conference on Computer Vision and Pattern Recognition. pp. 17452–17462 (2022)
26. Li, H., Trocan, M., Sawan, M., Galayko, D.: Cswin2sr: Circular swin2sr for compressed image super-resolution. arXiv preprint arXiv:2301.08749 (2023)
27. Li, X.L., Liang, P.: Prefix-tuning: Optimizing continuous prompts for generation. arXiv preprint arXiv:2101.00190 (2021)
28. Li, X., Jin, X., Fu, J., Yu, X., Tong, B., Chen, Z.: Few-shot real image restoration via distortion-relation guided transfer learning. arXiv preprint arXiv:2111.13078 (2021)
29. Li, X., Ren, Y., Jin, X., Lan, C., Wang, X., Zeng, W., Wang, X., Chen, Z.: Diffusion models for image restoration and enhancement—a comprehensive survey. arXiv preprint arXiv:2308.09388 (2023)
30. Li, X., Shi, J., Chen, Z.: Task-driven semantic coding via reinforcement learning. *IEEE Transactions on Image Processing* **30**, 6307–6320 (2021)
31. Li, X., Sun, S., Zhang, Z., Chen, Z.: Multi-scale grouped dense network for vvc intra coding. In: Proceedings of the IEEE/CVF Conference on Computer Vision and Pattern Recognition Workshops. pp. 158–159 (2020)
32. Li, Z., Lei, Y., Ma, C., Zhang, J., Shan, H.: Prompt-in-prompt learning for universal image restoration. arXiv preprint arXiv:2312.05038 (2023)
33. Lian, D., Yu, Z., Sun, X., Gao, S.: As-mlp: An axial shifted mlp architecture for vision. arXiv preprint arXiv:2107.08391 (2021)

34. Liang, J., Cao, J., Sun, G., Zhang, K., Van Gool, L., Timofte, R.: Swinir: Image restoration using swin transformer. In: Proceedings of the IEEE/CVF international conference on computer vision. pp. 1833–1844 (2021)
35. Liang, Z., Li, C., Zhou, S., Feng, R., Loy, C.C.: Iterative prompt learning for unsupervised backlit image enhancement. In: Proceedings of the IEEE/CVF International Conference on Computer Vision. pp. 8094–8103 (2023)
36. Liu, Z., Hu, H., Lin, Y., Yao, Z., Xie, Z., Wei, Y., Ning, J., Cao, Y., Zhang, Z., Dong, L., et al.: Swin transformer v2: Scaling up capacity and resolution. In: Proceedings of the IEEE/CVF conference on computer vision and pattern recognition. pp. 12009–12019 (2022)
37. Liu, Z., Lin, Y., Cao, Y., Hu, H., Wei, Y., Zhang, Z., Lin, S., Guo, B.: Swin transformer: Hierarchical vision transformer using shifted windows. In: Proceedings of the IEEE/CVF international conference on computer vision. pp. 10012–10022 (2021)
38. Luo, Z., Gustafsson, F.K., Zhao, Z., Sjölund, J., Schön, T.B.: Controlling vision-language models for universal image restoration. arXiv preprint arXiv:2310.01018 (2023)
39. Ma, J., Cheng, T., Wang, G., Zhang, Q., Wang, X., Zhang, L.: Prores: Exploring degradation-aware visual prompt for universal image restoration. arXiv preprint arXiv:2306.13653 (2023)
40. Martin, D., Fowlkes, C., Tal, D., Malik, J.: A database of human segmented natural images and its application to evaluating segmentation algorithms and measuring ecological statistics. In: Proceedings Eighth IEEE International Conference on Computer Vision. ICCV 2001. vol. 2, pp. 416–423. IEEE (2001)
41. Matsui, Y., Ito, K., Aramaki, Y., Fujimoto, A., Ogawa, T., Yamasaki, T., Aizawa, K.: Sketch-based manga retrieval using manga109 dataset. *Multimedia Tools and Applications* **76**(20), 21811–21838 (2017)
42. Mentzer, F., Toderici, G.D., Tschannen, M., Agustsson, E.: High-fidelity generative image compression. *Advances in Neural Information Processing Systems* **33**, 11913–11924 (2020)
43. OpenAI: Gpt-4 technical report (2023)
44. Park, T., Liu, M.Y., Wang, T.C., Zhu, J.Y.: Semantic image synthesis with spatially-adaptive normalization. In: Proceedings of the IEEE/CVF conference on computer vision and pattern recognition. pp. 2337–2346 (2019)
45. Potlapalli, V., Zamir, S.W., Khan, S., Khan, F.S.: Promptir: Prompting for all-in-one blind image restoration. arXiv preprint arXiv:2306.13090 (2023)
46. Qin, X., Zhu, Y., Li, C., Wang, P., Cheng, J.: Cidbnet: a consecutively-interactive dual-branch network for jpeg compressed image super-resolution. In: Computer Vision–ECCV 2022 Workshops: Tel Aviv, Israel, October 23–27, 2022, Proceedings, Part II. pp. 458–474. Springer (2023)
47. Sohn, K., Chang, H., Lezama, J., Polania, L., Zhang, H., Hao, Y., Essa, I., Jiang, L.: Visual prompt tuning for generative transfer learning. In: Proceedings of the IEEE/CVF Conference on Computer Vision and Pattern Recognition. pp. 19840–19851 (2023)
48. Su, C., Yang, F., Zhang, S., Tian, Q., Davis, L.S., Gao, W.: Multi-task learning with low rank attribute embedding for person re-identification. In: Proceedings of the IEEE international conference on computer vision. pp. 3739–3747 (2015)
49. Sullivan, G.J., Ohm, J.R., Han, W.J., Wiegand, T.: Overview of the high efficiency video coding (hevc) standard. *IEEE Transactions on circuits and systems for video technology* **22**(12), 1649–1668 (2012)

50. Sun, H., Li, W., Liu, J., Chen, H., Pei, R., Zou, X., Yan, Y., Yang, Y.: Coser: Bridging image and language for cognitive super-resolution. arXiv preprint arXiv:2311.16512 (2023)
51. Tang, C., Zhao, Y., Wang, G., Luo, C., Xie, W., Zeng, W.: Sparse mlp for image recognition: Is self-attention really necessary? In: Proceedings of the AAAI Conference on Artificial Intelligence. vol. 36, pp. 2344–2351 (2022)
52. Tang, Y., Han, K., Guo, J., Xu, C., Li, Y., Xu, C., Wang, Y.: An image patch is a wave: Phase-aware vision mlp. In: Proceedings of the IEEE/CVF Conference on Computer Vision and Pattern Recognition. pp. 10935–10944 (2022)
53. Timofte, R., Agustsson, E., Van Gool, L., Yang, M.H., Zhang, L.: Ntire 2017 challenge on single image super-resolution: Methods and results. In: Proceedings of the IEEE conference on computer vision and pattern recognition workshops. pp. 114–125 (2017)
54. Tolstikhin, I.O., Houlsby, N., Kolesnikov, A., Beyer, L., Zhai, X., Unterthiner, T., Yung, J., Steiner, A., Keysers, D., Uszkoreit, J., et al.: Mlp-mixer: An all-mlp architecture for vision. *Advances in neural information processing systems* **34**, 24261–24272 (2021)
55. Touvron, H., Bojanowski, P., Caron, M., Cord, M., El-Nouby, A., Grave, E., Izacard, G., Joulin, A., Synnaeve, G., Verbeek, J., et al.: Resmlp: Feedforward networks for image classification with data-efficient training. *IEEE Transactions on Pattern Analysis and Machine Intelligence* (2022)
56. Tu, Z., Talebi, H., Zhang, H., Yang, F., Milanfar, P., Bovik, A., Li, Y.: Maxim: Multi-axis mlp for image processing. In: Proceedings of the IEEE/CVF Conference on Computer Vision and Pattern Recognition. pp. 5769–5780 (2022)
57. Vandenhende, S.: Multi-task learning for visual scene understanding. arXiv preprint arXiv:2203.14896 (2022)
58. Vandenhende, S., Georgoulis, S., Van Gool, L.: Mti-net: Multi-scale task interaction networks for multi-task learning. In: *Computer Vision—ECCV 2020: 16th European Conference, Glasgow, UK, August 23–28, 2020, Proceedings, Part IV* 16. pp. 527–543. Springer (2020)
59. Wallace, G.K.: The jpeg still picture compression standard. *Communications of the ACM* **34**(4), 30–44 (1991)
60. Wang, J., Yue, Z., Zhou, S., Chan, K.C., Loy, C.C.: Exploiting diffusion prior for real-world image super-resolution. arXiv preprint arXiv:2305.07015 (2023)
61. Wang, T., Lu, W., Zhang, K., Luo, W., Kim, T.K., Lu, T., Li, H., Yang, M.H.: Promptrr: Diffusion models as prompt generators for single image reflection removal. arXiv preprint arXiv:2402.02374 (2024)
62. Wang, X., Xie, L., Dong, C., Shan, Y.: Real-esrgan: Training real-world blind super-resolution with pure synthetic data. In: Proceedings of the IEEE/CVF international conference on computer vision. pp. 1905–1914 (2021)
63. Wang, X., Yu, K., Wu, S., Gu, J., Liu, Y., Dong, C., Qiao, Y., Change Loy, C.: Esrgan: Enhanced super-resolution generative adversarial networks. In: Proceedings of the European conference on computer vision (ECCV) workshops. pp. 0–0 (2018)
64. Wei, G., Zhang, Z., Lan, C., Lu, Y., Chen, Z.: Activemlp: An mlp-like architecture with active token mixer. arXiv preprint arXiv:2203.06108 (2022)
65. Wu, R., Yang, T., Sun, L., Zhang, Z., Li, S., Zhang, L.: Seesr: Towards semantics-aware real-world image super-resolution. arXiv preprint arXiv:2311.16518 (2023)
66. Wu, Y., Li, X., Zhang, Z., Jin, X., Chen, Z.: Learned block-based hybrid image compression. *IEEE Transactions on Circuits and Systems for Video Technology* **32**(6), 3978–3990 (2021)

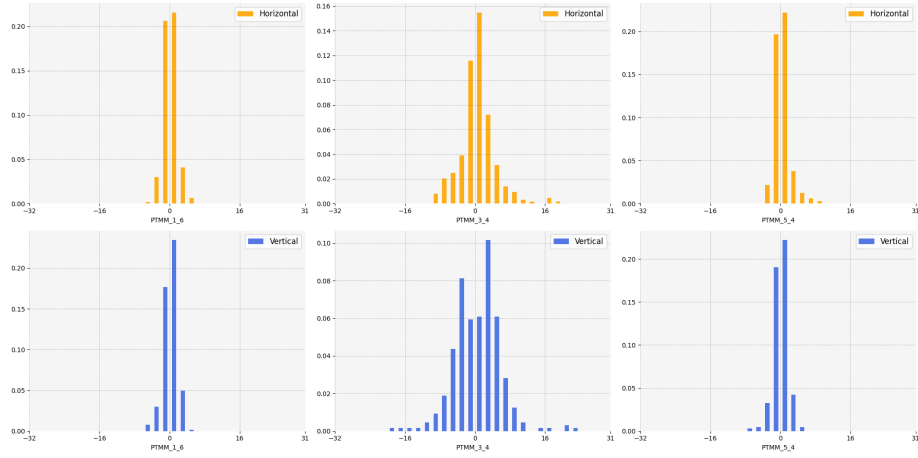
67. Yang, R., Timofte, R., Li, X., Zhang, Q., Zhang, L., Liu, F., He, D., Li, F., Zheng, H., Yuan, W., et al.: Aim 2022 challenge on super-resolution of compressed image and video: Dataset, methods and results. In: Computer Vision–ECCV 2022 Workshops: Tel Aviv, Israel, October 23–27, 2022, Proceedings, Part III. pp. 174–202. Springer (2023)
68. Yu, T., Li, X., Cai, Y., Sun, M., Li, P.: S2-mlp: Spatial-shift mlp architecture for vision. In: Proceedings of the IEEE/CVF Winter Conference on Applications of Computer Vision. pp. 297–306 (2022)
69. Zeyde, R., Elad, M., Protter, M.: On single image scale-up using sparse-representations. In: International conference on curves and surfaces. pp. 711–730. Springer (2010)
70. Zhang, D.J., Li, K., Chen, Y., Wang, Y., Chandra, S., Qiao, Y., Liu, L., Shou, M.Z.: Morphmlp: A self-attention free, mlp-like backbone for image and video. arXiv preprint arXiv:2111.12527 (2021)
71. Zhang, Y., Li, K., Li, K., Wang, L., Zhong, B., Fu, Y.: Image super-resolution using very deep residual channel attention networks. In: Proceedings of the European conference on computer vision (ECCV). pp. 286–301 (2018)

Appendix

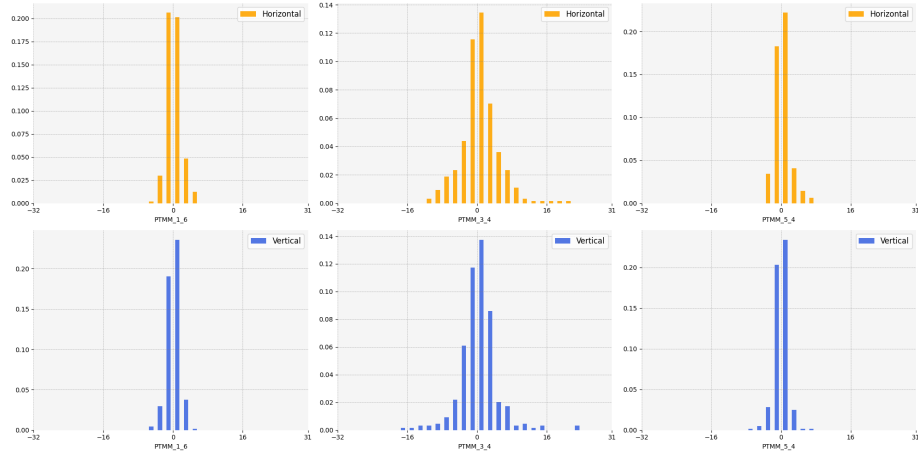
Section 6 illustrates the distribution of offsets from different PTMMs and codecs. Section 7 presents more qualitative results on various compression codecs and qualities.

6 Distribution of Offsets

We investigate the learned distributions of offsets via histogram visualization of offsets from different Prompt guided Token Mixer Modules (PTMMs). The i and j of PTMM $_i_j$ denotes the offsets of j^{th} PTMM from i^{th} PTMM. We have the following observations: 1) As the depth increases, the learned offsets first expand to a larger range and then shrink to a smaller range. This hints that the model learns to extract local information for the query token at shallow layers. In the middle layers, the model leverages the offsets to aggregate the global-wise information to perform better token mixing. At the last layers, the distortions contained in image features are mostly removed, therefore the model focuses more on using local information again to refine the query tokens for the reconstruction purpose. 2) The distribution of offsets from middle layers differs among various codecs. We attribute this to the guidance from task-specific prompts. Since the distortion varies among different codecs, the visualization of learned offsets validates that our prompts are capable of providing adaptive guidance against various distortions, thus leading to better performance in the CSR tasks [24, 67]. 3) The offsets expand to a wider range for learning-based codecs compared to traditional codecs. We believe this is because the distortion introduced by learning-based codecs is more challenging to eliminate compared to that from traditional codecs, necessitating broader ranges of offsets to extract useful information for query tokens.

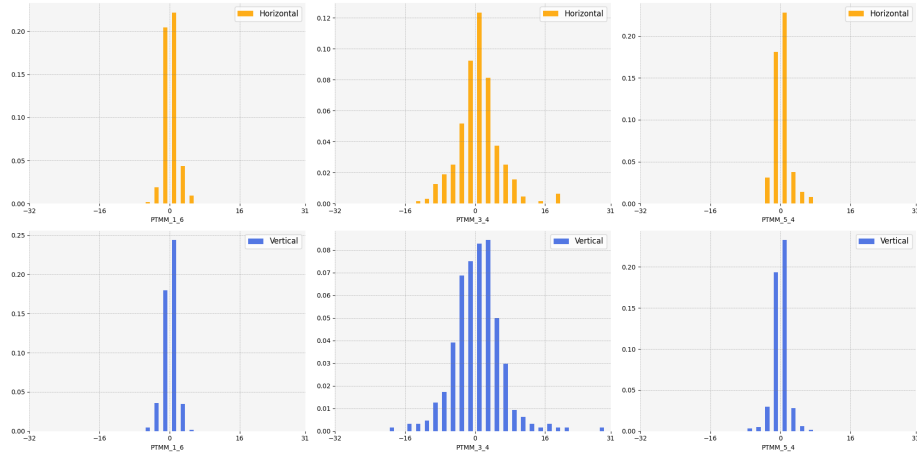
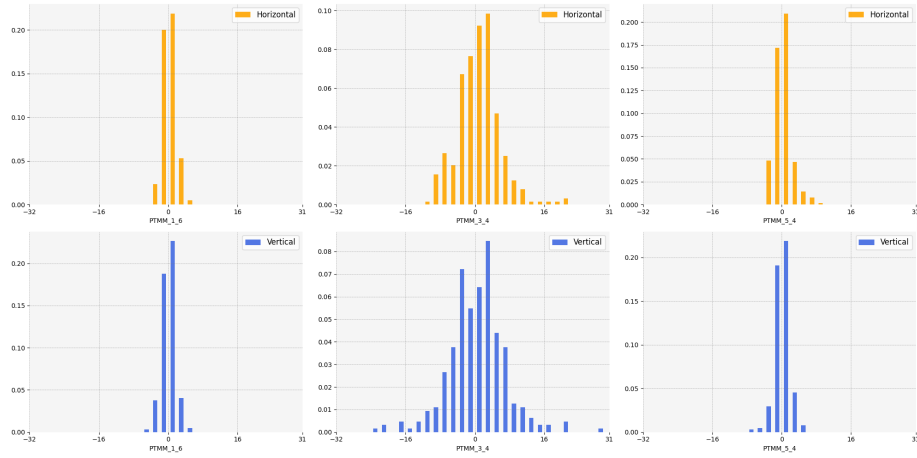


(a) Visualization of learned offsets for JPEG [59].



(b) Visualization of learned offsets for VTM [5].

Fig. 5: Histograms of learned offsets for the center token from different PTMMs. LR images are randomly sampled from Urban100 [19] compressed by C_{PSNR} [9] and VTM [5] codecs.

(a) Visualization of learned offsets for C_{FSNR} [9].

(b) Visualization of learned offsets for HIFIC [42].

Fig. 6: Histograms of learned offsets for the center token from different PTMMs. LR images are randomly sampled from Urban100 [19] compressed by JPEG [59] and HIFIC [42] codecs.

7 More Visual Results

We provide more visual comparisons between our UCIP with state-of-the-art methods on different codecs and different compression qualities within a single codec. UCIP shows clearer textures and less artifacts in super-resolved images, indicating that our prompts and offsets are adaptive and robust against various degradations.



Fig. 7: Visual Comparisons between UCIP and other methods on HIFIC ($Q = \text{'high'}$) from Urban100 [19].



Fig. 8: Visual Comparisons between UCIP and other methods on $HM(Q = 32)$ from Urban100 [19].

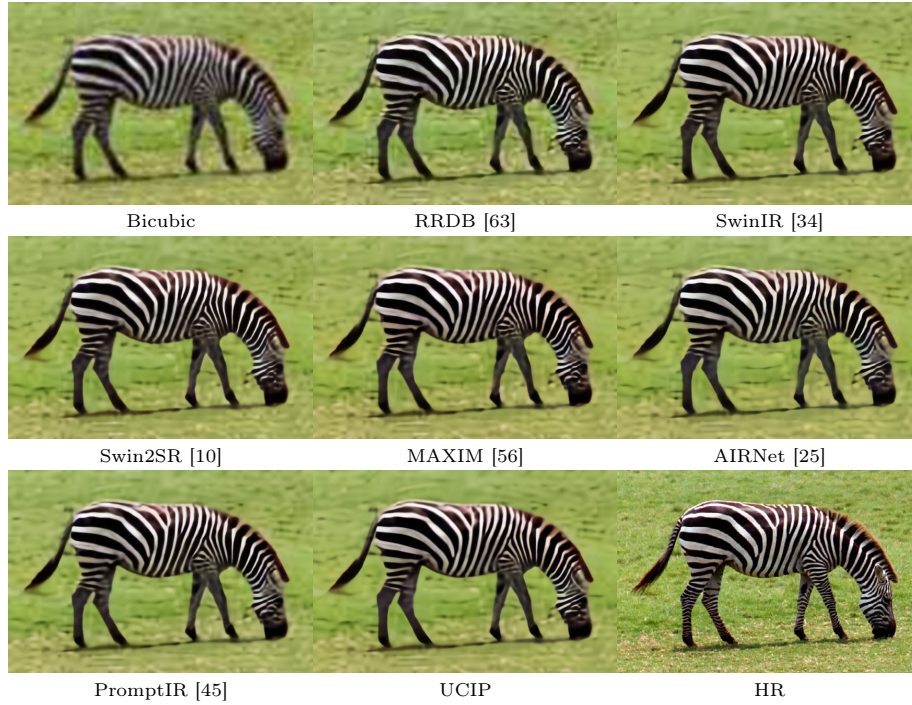


Fig. 9: Visual Comparisons between UCIP and other methods on JPEG ($Q = 30$) from Set14 [69].

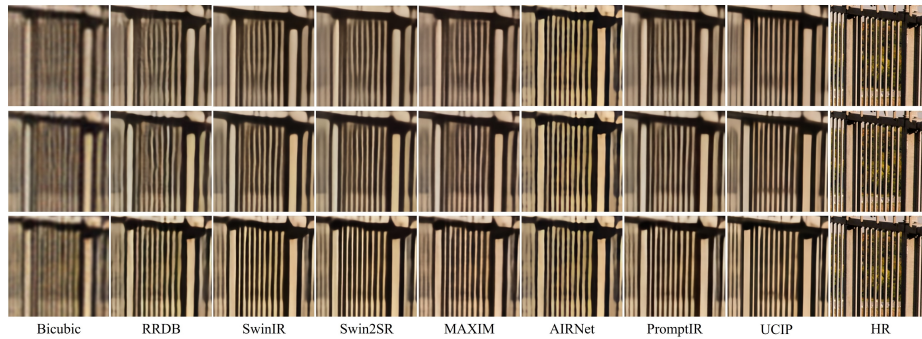


Fig. 10: Visual comparisons between UCIP and other state-of-the-art methods under different compression qualities within HIFIC [42] codec. The qualities of HIFIC from top to bottom are ‘low’, ‘medium’, and ‘high’, respectively.